Remotely Controlled Continuous Surveillance of Viral RNA in Wastewater Using a LoRa Network

Aneesh Kshirsagar, *Member, IEEE*, Anthony J. Politza, Ming Dong, and Weihua Guan, *Senior Member, IEEE*

***Abstract*—Tracking the rapid spread of infectious diseases, such as COVID-19, in communities poses a significant global health challenge, mainly because traditional testing methods struggle to detect asymptomatic carriers and effectively manage outbreaks. To address this, we present a scalable, networked molecular testing framework for wastewater-based epidemiology (WBE) that, for the first time, integrates portable nucleic acid testing (NAT) devices with long-range (LoRa) wireless communication and cloud-based data management. Each battery-powered node can perform reverse transcription–loop-mediated isothermal amplification (RT-LAMP), a rapid nucleic acid amplification method, on-site directly on raw wastewater samples for SARS-CoV-2 detection. A node executes up to eight independent tests on a microfluidic cartridge, monitoring fluorescence signals from the RT-LAMP reactions in real time and transmitting the results via LoRa radio to a gateway, which uploads structured data to a NoSQL cloud database. An interactive dashboard enables bidirectional communication with nodes and provides spatiotemporal visualization of both live and historical data, including hotspot identification through geotagging and mapping of metrics such as seven-day positivity rates. Rigorous system testing with four nodes under varied transmission scenarios confirmed a packet delivery ratio (PDR) exceeding 99%, ensuring accurate and reliable reconstruction of time-series RT-LAMP curves. By integrating NAT with IoT communication and cloud analytics, this system supports unattended, long-term wastewater monitoring and can provide public health officials with timely, actionable insights. This framework demonstrates the potential of IoT-enabled molecular testing to advance decentralized surveillance beyond conventional laboratory-based workflows.**

***Index Terms*—Long range (LoRa) radio, networked nucleic acid testing (NAT), SARS-CoV-2, wastewater epidemiology.**

Received 1 April 2025; revised 26 August 2025 and 14 December 2025; accepted 30 December 2025. Date of publication 6 January 2026; date of current version 9 March 2026. This work was supported in part by the National Institutes of Health under Grant R33AI147419, in part by the National Science Foundation under Grant 2319913, and in part by American RescueAct through United States Department of Agriculture (USDA) Animal and Plant Health Inspection Service (APHIS) (APHIS/National Institute of Food and Agriculture (NIFA) Collaborative) under Award 2023-70432-41395). *(Corresponding author: Weihua Guan.)*

Aneesh Kshirsagar and Weihua Guan are with the Department of Intelligent Systems Engineering, Luddy School of Informatics, Computing, and Engineering, Indiana University, Bloomington, IN 47405 USA (e-mail: anekshir@iu.edu; guanw@iu.edu).

Anthony J. Politza is with the Department of Biomedical Engineering, The Pennsylvania State University, University Park, PA 16802 USA (e-mail: ajp6126@psu.edu).

Ming Dong is with the Department of Electrical Engineering, The Pennsylvania State University, University Park, PA 16802 USA (e-mail: mkd5669@psu.edu).

This article has supplementary downloadable material available at https://doi.org/10.1109/JIOT.2026.3651506, provided by the authors.

Digital Object Identifier 10.1109/JIOT.2026.3651506

I. Introduction

THE effective management of infectious diseases depends heavily on the ability to detect and monitor viral presence within populations [1]. Traditional diagnostic methods, such as individual testing of symptomatic carriers, often fall short, missing asymptomatic and mildly symptomatic individuals who could contribute significantly to the spread of infections [2], [3]. This underdiagnosis is particularly problematic in resource-limited settings, where the availability of testing is often insufficient to accurately gauge the true prevalence of a disease [4], [5].

Wastewater-based epidemiology (WBE) emerges as a robust alternative, offering a comprehensive method for monitoring viral spread within communities [6], [7]. This approach involves analyzing wastewater to detect viral RNA and has shown a promising correlation with clinical findings from nasal swabs. For instance, studies in various metropolitan areas have demonstrated that increases in SARS-CoV-2 RNA loads in wastewater precede spikes in COVID-19 clinical cases, providing an early warning of outbreak escalations [8], [9], [10], [11]. Moreover, wastewater surveillance facilitates the early detection of virus variants and trends in prevalence, often providing insights up to two weeks before these are observable in clinical data [12]. This capability is invaluable for public health officials and policymakers, who can implement timely interventions based on these early indicators. In addition, wastewater surveillance offers a resource-efficient alternative to individual testing, making it particularly valuable for long-term monitoring in regions with limited healthcare infrastructure [13]. Its implementation in ongoing health monitoring can significantly enhance public health responsiveness without the extensive resource allocation required for individual tests.

The current state-of-the-art WBE relies heavily on established sample collection, transportation, and analysis protocols [14], [15], [16]. Samples are generally collected from various wastewater sources and require preservation during transport to prevent RNA degradation [17], [18]. This is typically achieved through cold chain logistics, where samples are kept at low temperatures to maintain integrity, which is crucial for the accuracy of downstream molecular analyses. Thus, the workflow from collection to analysis is labor-intensive, with samples needing to be physically collected and transported by personnel to centralized laboratories, which can be a significant bottleneck, especially when scaling up extensive geographic surveillance. The laborious nature of this grab-sample step emphasizes the need for a high degree of

coordination and can lead to delays in sample processing and analysis.

Upon arrival at the laboratory, viral pathogens are detected in the wastewater samples through polymerase chain reaction (PCR) molecular testing [19]. While PCR is regarded for its sensitivity and specificity and has been used extensively for WBE for SARS-CoV-2, another process that may either be used in conjunction with PCR or on its own is next generation sequencing (NGS) for a more detailed analysis [12], [20], [21]. Metagenomic NGS allows for sequencing the entire genetic material in the samples, providing insights into the presence of SARS-CoV-2 and its variants. This method can track the evolution of the virus and identify new mutations as they occur in the population. However, PCR and NGS require additional elaborate sample preparation steps, including RNA purification and library preparation (in the case of sequencing), to meet the sample quality requirements for downstream analysis. Thus, existing WBE efforts largely depend on centralized laboratory testing, which typically involves sample collection and transport. While these methods provide sensitive results, they are resource-intensive, require specialized personnel, expensive instruments, and have long turnaround times (48–96 h), and do not enable unattended and persistent monitoring.

We have previously developed several standalone point-of-need portable nucleic acid amplification instruments for clinical diagnostic purposes [22], [23], [24], [25]; however, these do not have networking capabilities beyond Bluetooth connectivity with a smartphone app. Recent efforts have explored portable and decentralized nucleic acid detection of SARS-CoV-2 in wastewater, including the RT-LAMP-*PfAgo* assay in a portable instrument [26], RT-LAMP assay on the MINI device [27], and QPsor, a Nanotrap microbiome particle and RNA isothermal coassisted and coupled amplification (RICCA)-based assay combined with paper-based lateral flow readout [28]. While these platforms demonstrate the feasibility of in-field wastewater testing, they are limited to isolated, manually operated assays and do not support long-term, networked deployment. In parallel, long-range (LoRa)-based wireless sensor networks have been widely applied in environmental monitoring, including air quality [29], [30], water quality [31], [32], and smart agriculture [33]. These studies demonstrate the scalability and low-power benefits of LoRa for distributed sensing applications. However, these examples have focused on physical and chemical parameters rather than molecular detection. This highlights a critical unmet need for a scalable, autonomous, real-time surveillance system that can provide spatiotemporal nucleic acid amplification data for WBE without the logistical and resource constraints of centralized laboratory workflows.

This article addresses this significant gap in WBE by developing a networked nucleic acid testing (NAT) platform to perform on-site testing of raw wastewater samples for the presence of SARS-CoV-2 RNA. The node is a portable battery-powered device equipped with eight NAT chambers that support multispectral monitoring of reverse transcription–loop-mediated isothermal amplification (RT-LAMP), an integrated GPS, and LoRa communication, making it a comprehensive tool for molecular testing of SARS-CoV-2 in wastewater

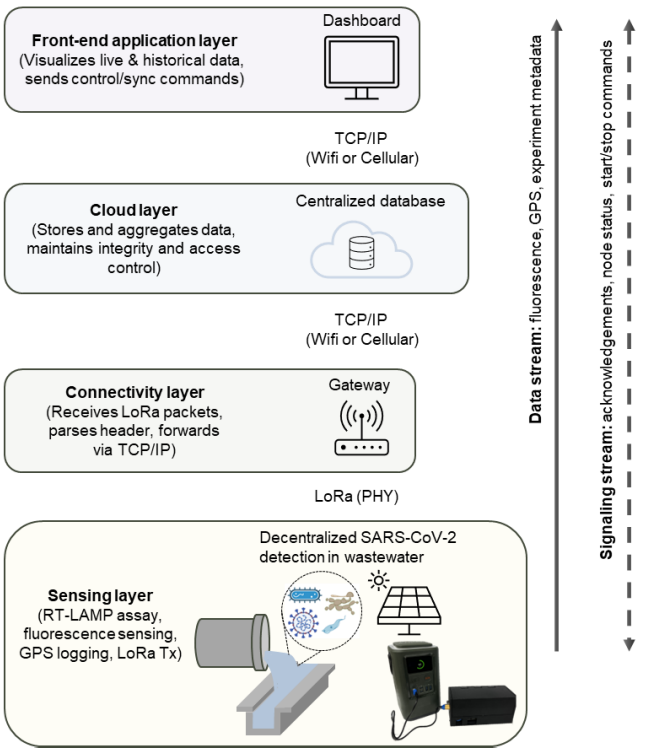

Fig. 1. Architecture of the networked wastewater surveillance platform is organized into four functional layers: 1) sensing layer, which includes portable, battery- or solar-powered nodes that perform on-site RT-LAMP assays, collect fluorescence and GPS data, and transmit processed results over LoRa; 2) connectivity layer, comprising gateways that aggregate LoRa packets, identify transmitting nodes, and forward structured data to the cloud; 3) cloud layer, which ensures scalable storage, data management, and integrity; and 4) application layer, which provides an interactive dashboard for real-time visualization and spatiotemporal trend analysis of SARS-CoV-2 RNA in wastewater. The solid arrow denotes the data stream (fluorescence, GPS, and metadata) flowing upward from nodes to the dashboard, while the dashed arrow denotes the signaling stream (control, synchronization, and acknowledgment messages) enabling coordination between the cloud and distributed devices.

with high sensitivity directly at the wastewater sites, and represents a transformative advancement in public health surveillance. Furthermore, connecting multiple such nodes in a scalable network facilitates real-time data transmission over extended ranges, enhancing the rapid collection and analysis of spatiotemporal data. This setup eliminates the traditional dependencies on manual sample collection and centralized laboratory processing. Cloud-based data management and dashboard deployment also support extensive data analysis capabilities, including real-time amplification curve monitoring and historical data evaluation. This contribution could be far-reaching, offering a scalable, efficient, and technologically advanced solution that could impact global health, particularly in managing and mitigating the spread of infectious diseases through timely and accurate wastewater surveillance.

II. Overview of the Networked Surveillance System

To address the need for quick and decentralized real-time wastewater monitoring for the presence of SARS-CoV-2 RNA, we developed an integrated, scalable, and networked NAT

platform. Fig. 1 illustrates functional framework of the system, organized into four layers. The *sensing layer* comprises a portable, battery-powered node designed for on-site nucleic acid detection using RT-LAMP assay [34], [35]. Each node independently processes wastewater samples and transmits results wirelessly over LoRa communication. Although a single node is shown for simplicity, the system is designed to support multiple nodes deployed across different locations. The *connectivity layer* includes gateways that aggregate radio packets from multiple nodes, identify their source IDs, and forward structured data to the cloud via TCP/IP. The *cloud layer* provides scalable data management, ensuring secure storage, data integrity, and accessibility. The *application layer* provides a front-end dashboard (https://aneksh-ionat.web.app) that visualizes live and historical results, provides spatiotemporal tracking, and enables public health officials to monitor ongoing tests, issue configuration updates, and make informed decisions. Thus, within the overall framework, four functional modules exist: 1) nodes, which perform on-site RT-LAMP assays, collect fluorescence and GPS data, and initiate wireless transmission; 2) gateway, which parses radio messages and forward structured data to the cloud; 3) Google Firestore, a NoSQL cloud database, which provides scalable storage, data integrity, and secure access; and 4) dashboard hosted on Google Firebase, which retrieves and visualizes spatiotemporal data. Furthermore, two complementary information flows have been established. The *data stream* (solid arrows) carries time-series fluorescence intensities, GPS coordinates, and experiment metadata from nodes to the dashboard through the gateway and cloud. The *signaling stream* (dashed arrows) conveys control, synchronization, node status, and acknowledgment messages, enabling bidirectional interaction between the user interface and field-deployed devices. Together, these modules and information flows constitute a cohesive architecture that supports reliable, scalable, and real-time wastewater surveillance.

Key features of the system include immediate on-site testing, portability, LoRa wireless communication, and independence from cold-chain transportation and centralized laboratory processing. These features significantly enhance scalability, deployment flexibility, and operational efficiency, making the system suitable for widespread adoption. Section III details the experimental setup, including the design and fabrication of the node and its modules, the RT-LAMP assay conditions, the LoRa network configuration, and the data management/dashboard framework. These descriptions provide the necessary context for Section IV, where the performance of each component and the overall system is evaluated. Conclusions and future research directions are discussed in Section V.

III. Experimental Setup

A. Node Design and Fabrication

To achieve decentralized wastewater monitoring, the proposed network requires nodes that can operate independently, transmit data wirelessly, and integrate seamlessly with cloud-based storage and visualization systems. Fig. 2(a) depicts an exploded view of the node built around a Raspberry Pi Zero, measuring 168 mm in length, 70 mm in width, and 80 mm in height. A 3-D-printed enclosure consists of a base for attaching the control printed circuit board (PCB) and a top section that houses additional PCBs, a heating block, and a microfluidic cartridge, with a hinged lid for accessing internal components. A single switch controls power, which is supplied by a large external battery pack that can be charged via a solar panel. The electronic block diagram is shown in Supplementary Fig. S1.

1) *Microfluidic Cartridge:* Fig. 2(b) shows the microfluidic cartridge designed to intake wastewater using the piezo pump suction. The wastewater flows in a U-shaped channel and encounters a semicircular isolation chamber that meters and dispenses a 10-μL sample into the underlying cylindrical reaction chamber, which is preloaded with RT-LAMP reagents. The workings of this dispensing mechanism and cartridge fabrication have been discussed [22], and the piezo pump has been characterized previously [34]. In addition, SARS-CoV-2 detection directly in raw wastewater with RT-LAMP has been validated when using a 5–10-μL sample in a 25-μL reaction [36], [37].
2) *Thermal Module:* As shown in Fig. 2(a), hollow cuboidal aluminum structures are mounted onto an acrylic backplate using epoxy resin, allowing for easy mounting and providing structural support while enabling individual thermal control for each chamber. These aluminum structures enclose the cartridge's reaction chambers on five sides, ensuring it precisely fits into the recesses for optimal heat transfer, thereby providing uniform, quick, and consistent heating of the RT-LAMP reagents while minimizing variation among chambers and across multiple experiments. Power resistors are attached using thermally conductive adhesive paste to generate heat.
3) *Optical Module:* The RT-LAMP reaction reagents include a fluorescent dye, SYTO-9, which intercalates into the double-stranded amplicons produced as the reaction product, and the fluorescence intensity increases as the reaction proceeds if the intended target (in this case, SARS-CoV-2 RNA) is present. To monitor the emitted fluorescence in real time, the optical module shown in Fig. 2(c) comprises a blue excitation LED strategically positioned on the back of the heating block, which directs light through a fabricated hole into the reaction chamber. Potentiometers enable manual fine-tuning of the LED current, complemented by PWM control for coarse adjustments. The optical system also includes an AS7341 spectral sensor to measure the emissions from the reaction chamber. These sensors improve fluorescence detection capabilities by measuring light across eight discrete visible-wavelength channels [38]. Because the AS7341 sensors have fixed, nonconfigurable I^2C addresses, a TCA9548A 1-to-8 I^2C multiplexer is used to interface the eight parallel sensors to the Raspberry Pi Zero.

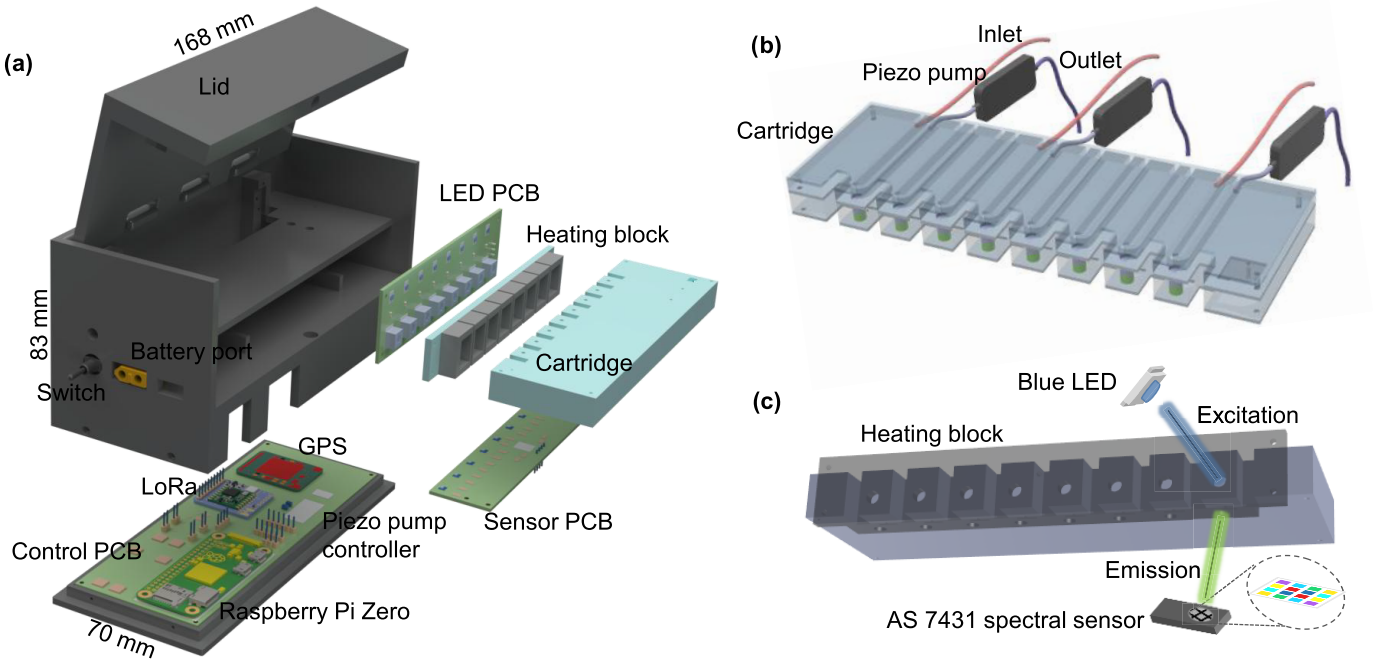

Fig. 2. Design and validation of the node. (a) Exploded view shows the base housing all the major electronic components and the top case with a shelf to slide the cartridge, which fits into the heating block. (b) Microfluidic cartridge for wastewater sampling and RT-LAMP testing. A piezo pump draws the sample through an inlet tube, isolates a droplet in the metering chamber, and deposits it into the reaction chamber while the excess sample exits via the outlet tube. The pump is connected to the cartridge via a Luer lock for easy assembly and disassembly. Cartridges support up to eight tests, with only three pump assemblies shown for simplicity. (c) Optical assembly for fluorescence detection: a blue LED excites reaction reagents through an opening in the heating block, while a spectral sensor captures the resulting emission through another opening.

4) *Communication Module:* LoRa was used for wireless data transmission, enabling low-power, LoRa communication in the decentralized wastewater monitoring setup. The Adafruit RFM96W LoRa Radio Transceiver, operating at 433 MHz and based on the SX1276 chip, interfaces with the Raspberry Pi Zero via Serial Peripheral Interface (SPI), ensuring reliable integration for data transmission. It features adjustable power output ranging from +5 to +23 dBm (up to 100 mW), allowing deployment-specific optimization. The module supports both simple wire antennas and external active antennas via U.FL or SMA connectors to balance power efficiency and communication reliability based on environmental conditions and deployment requirements.
5) *Localization Module:* Integrating GPS into the wastewater monitoring system enables real-time spatiotemporal data mapping, essential for associating test results with specific locations and tracking the spread of infectious diseases. The Adafruit Ultimate GPS Breakout, based on the MediaTek GPS Chipset MT333, was selected for its easy USB integration into portable instruments, low cost, low power consumption, and excellent tracking sensitivity of −165 dBm. Despite its small form factor, the module provides sub-3-m position accuracy. In addition, its warm start capability, supported by a real-time clock (RTC) battery, ensures faster reacquisition of satellite signals following temporary power interruptions. The module also supports an external active antenna via a U.FL connector, which, if used, could significantly improve signal reception in challenging environments.
6) *Fabrication Details:* All structural parts were designed in SolidWorks CAD, while PCBs were designed in Eagle CAD. The housing was fabricated on a MakerBot MethodX 3-D printer using acrylonitrile butadiene styrene (ABS) material. The heating block was machined by Protolabs Network, and the PCBs were fabricated by OSH Park LLC. The heating block incorporates four 0.5-Ω power resistors (MP725-0.50), mounted with a thermally conductive adhesive paste (Arctic Alumina) and an MC65F103A 10-kΩ thermistor (Amphenol Thermometrics), positioned in a small recess for temperature feedback. All electronic components, such as the blue excitation LEDs (XZFBB78W), spectral sensors (AS7341), LoRa Radio module (Adafruit RFM96W), GPS module (Adafruit Ultimate GPS—PA1616S), Raspberry Pi Zero, power resistors, thermistor, and other passive components were purchased from DigiKey.com. The piezo pump (mp6-hyb) and its control circuitry (mp6-OEM), developed by Bartels Mikrotechnik, were purchased from Servoflo Corporation.

B. Network Implementation and LoRa Settings

For communication, each node incorporates an Adafruit RFM96W LoRa transceiver (433 MHz) interfaced to the onboard Raspberry Pi Zero via SPI using the Adafruit CircuitPython rfm9x library. Amplification-curve data were

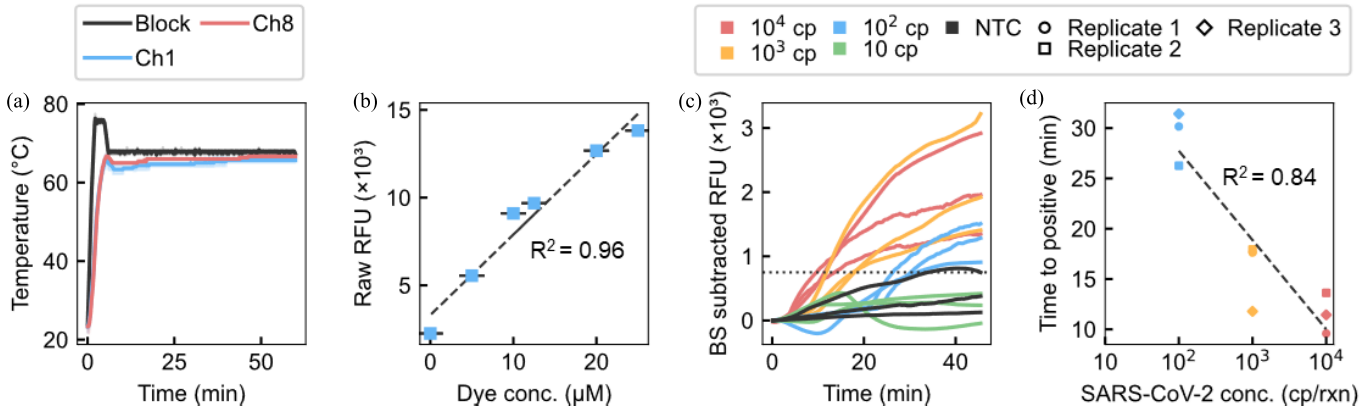

Fig. 3. Validation of key analyzer modules. (a) Temperature validation confirms that the reagents reach ~64 °C within 5 min and remain stable throughout the reaction time. (b) Optical module characterization reveals a linear relationship for increasing fluorescent dye concentration with $R^2 = 0.96$. (c) Real-time amplification curves for serially diluted SARS-CoV-2 RNA samples (from 10^4 to 10 cp/rxn) run in triplicate on the node. (d) Assay linearity: time-to-positive values plotted against RNA concentration, $R^2 = 0.84$ indicates moderate linearity.

transmitted as short payloads (~125 bytes per packet, below the 255-byte LoRa limit) during the hour-long assay, with one datapoint transmitted every 20 s. Transmission parameters were configured as follows: bandwidth of 125 kHz, spreading factor of SF7, coding rate of CR 4/5, and high-power mode with a target output of +23 dBm. CRC was enabled, and application-layer acknowledgments with retries were used to confirm packet-level delivery. The gateway was implemented on a Raspberry Pi 4B with an identical RFM96W transceiver; received packets were parsed and forwarded to a NoSQL cloud database using the Firebase Admin SDK. For performance analysis, the packet delivery ratio (PDR) was defined as the fraction of packets correctly decoded, parsed, and written to cloud storage (the final destination) relative to the total number of packets transmitted by the nodes. All transmissions complied with regional regulations for the 433 MHz ISM band (duty cycle and power limits).

C. RT-LAMP Assay

The RT-LAMP reaction mix comprised New England Biolabs (NEB) isothermal buffer (1×), SARS-CoV-2 N gene-specific primer set (0.2 μM for F3 and B3, 1.6 μM for FIP and BIP, 0.8 μM for LF and LB) manufactured by Integrated DNA Technologies (IDT), Betaine (0.6M), $MgSO_4$ (5 mM), SYTO-9 dye (3 μM), deoxyribonucleotide triphosphates (dNTPs, 1.4 mM), Bst 2.0 DNA polymerase (0.4 U/μL), Warmstart reverse transcriptase (0.3 U/μL), and either 10 μL of SARS-CoV-2 target (ATCC VR-1986HK) or a sample. PCR-grade H_2O was added to supplement the reaction to a volume of 25 μL. The assay was conducted at a constant temperature of approximately 64 °C. For further details, refer to Supplementary Tables S1 and S2.

D. Cloud Storage, Dashboard Programming, and Hosting

The dashboard and associated functionalities were developed using PyCharm IDE, employing Node.js for backend operations and HTML for the frontend interface. Google Firestore, a NoSQL database, was used for data storage, with database operations supported by the Firebase Admin SDK, including read and write operations. Google Firebase hosting was used to deploy the dashboard and other features, including dynamic data aggregation and analysis, ensuring seamless data handling between the dashboard and Firestore.

IV. Results and Discussion

A. Validation of Key Node Modules

1) Thermal Module Performance: Power resistors, which generate heat when current flows through them, are attached to the aluminum structures using a thermally adhesive paste, efficiently and quickly transferring the heat and raising the structure's temperatures to 76 °C within 2 min and maintaining it for 3 min so that the reagents reach approximately 64 °C within 5 min of initiating the heating [see Fig. 3(a)].

2) Optical Module Performance: Fig. 3(b) demonstrates the optical module's precision in measuring fluorescence emissions for increasing dye concentration and its effectiveness in monitoring LAMP reactions, achieving excellent linearity ($R^2 = 0.96$). Although data from all channels of the spectral sensor are recorded and transmitted, the channel centered at 515 nm, which is the most responsive for monitoring the RT-LAMP reaction using SYTO-9 fluorescent dye (peak emission: 498 nm), was selected to represent the relative fluorescence units (RFUs).

3) RT-LAMP Validation on the Node: To illustrate the use of our instrument, we used mock samples containing serially diluted (10×) purified SARS-CoV-2 RNA, ranging between 10^4 and 10 copies per reaction (cp/rxn). These samples were added to the RT-LAMP reaction mix, and the reactions were carried out on the microfluidic cartridge. Real-time amplification curves (in triplicate) for these samples, along with no-template control (NTC) reactions, are shown in Fig. 3(c). The corresponding time-to-positive values plotted against RNA concentration are shown in Fig. 3(d), yielding an R^2 of 0.84, which indicates moderate linearity and supports the system's qualitative detection capability. While a thorough and systematic evaluation using hit ratios for serially diluted samples is required to determine detection sensitivity, our previous studies that evaluated on-cartridge detection [22],

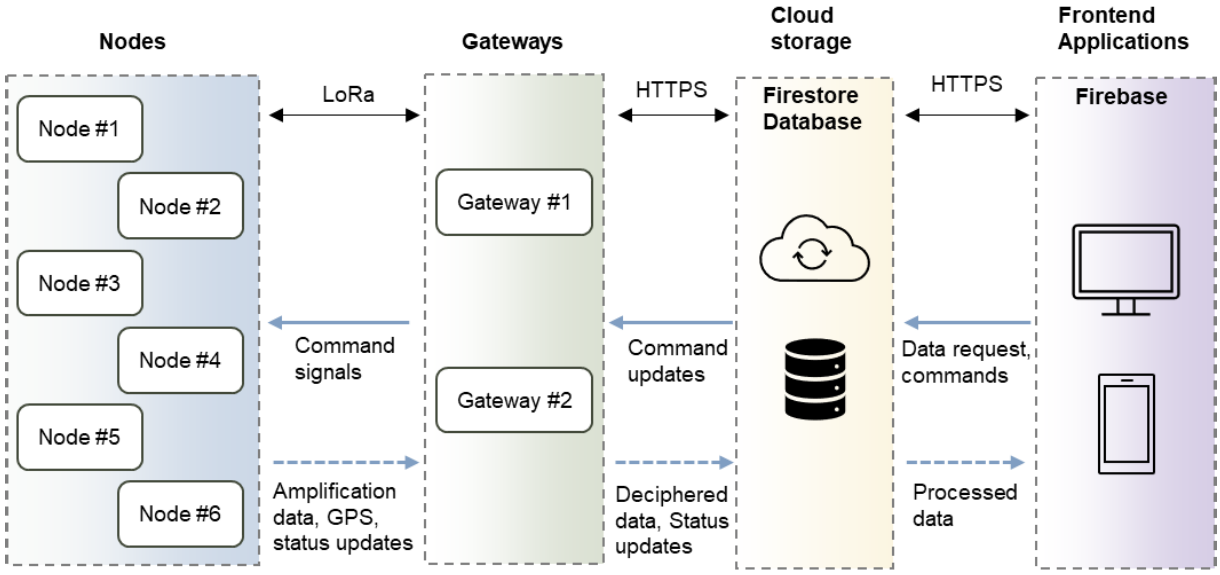

Fig. 4. Network architecture. The system comprises four primary components: end nodes, gateways, cloud storage, and frontend applications. Nodes transmit status updates, GPS, and real-time data via LoRa to a Raspberry Pi 4B-based gateway running the Firebase Admin SDK. The gateway deciphers messages, uploads data to Google Firebase, a cloud database, for efficient storage in collections and documents, and relays commands to nodes. Firebase enables real-time data upload and querying, which the dashboard hosted on Google Firestore retrieves to analyze and visualize as spatiotemporal trends and provide historical or live test monitoring. Commands, such as resetting the test counter or initiating new tests, are set via database flags. The gateway reads these flags, interprets them, and transmits corresponding LoRa messages to the nodes.

[34] and assay characterization [23] indicate that qualitative identification of SARS-CoV-2 is achievable within 60 min. Considering previously reported viral concentrations in raw wastewater, typically around 10 copies/μL of water [36], [39], [40], using a 10-μL sample per reaction (corresponding to 100 viral copies per reaction) places the node's sensitivity within the range required for wastewater testing. This demonstrates the instrument's suitability for deployment into a broader networked NAT framework for decentralized SARS-CoV-2 monitoring.

4) Power Consumption: The instrument's real-time power consumption during the RT-LAMP reaction [see Supplementary Fig. S1(d)] indicates a total energy consumption of approximately 5.2 Wh per 1-hour test, and the standby energy consumption is estimated at ~16 Wh per day. Using a commercially available 192 Wh Anker power station (pictured in Fig. 1), the system can operate for about eight days with one test per day. This aligns well with the microfluidic cartridge's capacity for eight tests, allowing the battery and cartridge to be replaced in a single operational trip if required. While a longer power backup would reduce the frequency of battery replacements, the ability to synchronize battery and cartridge replacement minimizes the logistical effort. In addition, the power station supports solar panel-based recharging, though this feature was not tested in the current study.

B. Network Architecture

LoRa, a proprietary wireless communication standard developed by Semtech, uses chirp spread spectrum (CSS) modulation, which enhances robustness to interference and enables LoRa communication capabilities at the cost of lower bandwidth. This trade-off makes LoRa particularly suitable for applications that require low-power, long range communication for transmitting small data packets, such as decentralized wastewater monitoring systems. The hierarchical architecture implemented in this study leverages LoRa's capability for reliable multinode communication in diverse environments, aligning with previous studies demonstrating its utility in field-deployed networks [41], [42], [43]. Fig. 4 illustrates the network architecture, showing the flow of information between its four primary components: end nodes, gateways, cloud storage, and frontend applications.

1) *End Nodes:* Each node collects real-time amplification data, GPS coordinates, and status updates during testing. These data are transmitted via LoRa to the gateway, ensuring efficient communication with minimal energy consumption.
2) *Gateways:* The gateway is a Raspberry Pi 4B equipped with a LoRa module to establish handshakes with the nodes and receive data. It runs the Firebase Admin SDK to enable secure communication with Firestore. The gateway aggregates incoming data from multiple nodes, deciphers LoRa packets, reformats the data into JSON objects, and uploads them to cloud storage via HTTPS. This configuration ensures data integrity, facilitates real-time updates, and enables bidirectional communication for real-time system control, such as sending command signals back to the nodes when required. For additional details on the gateway's design and functionality, refer to Supplementary Fig. S2.
3) *Cloud Storage:* Google Firebase, a part of Firestore, stores data received from gateways, ensuring scalability, secure access, and real-time querying. It serves as

the system's backbone for ensuring data integrity and facilitating spatiotemporal analysis.

4) *Frontend Applications:* This graphical user interface retrieves processed data from the cloud to provide users with an interactive dashboard. Users can visualize live or historical amplification data, monitor node status, and enable public health-related informed decisions or interventions using spatiotemporal data.

The modular design and low-bandwidth communication protocol enable the system to scale effectively, supporting up to 254 nodes per gateway, governed by the maximum number of unique IDs in the 8-bit addressing scheme of the CircuitPython library implementation, with address 255 reserved for broadcasting to all instead of targeting a specific node or gateway. Typical applications benefit from LoRa's communication capabilities, which extend several kilometers in rural areas with minimal obstructions, albeit at the expense of lower data rates. This is particularly advantageous for deploying large-scale distributed monitoring systems in remote areas or regions with limited infrastructure. In addition, network design eliminates the need for manual sample collection, significantly reducing delays and operational costs associated with centralized laboratory processing.

C. Data Transmission and Network Validation

Efficient and reliable communication between nodes and the gateway is fundamental to ensuring the integrity of real-time monitoring data, enabling precise spatiotemporal analysis and rapid diagnostic decision-making in decentralized surveillance networks. The nodes are programmed to send two types of messages to the gateway: data messages and meta messages. As shown in Fig. 5(a), fluorescence emissions from the reaction chamber track the reaction progress during the RT-LAMP reaction. These emissions, due to excitation by a blue LED, are captured by a spectral sensor across eight wavelength channels. The captured values are transmitted as RFU along with relative time, with readings taken every 20 s during the hour-long experiment. Data messages are identified by a header containing the node ID and message type, ensuring they can be processed appropriately by the gateway. Similarly, meta messages include headers that convey additional information, such as GPS coordinates or the node's status (e.g., readiness to begin an experiment). Both message types are structured to limit their size to approximately 125 bytes, well within the 255-byte theoretical maximum supported by the Semtech LoRa module.

Once received, the gateway running a Python script processes these messages and prepares them for upload and storage in Google Firestore, a NoSQL database, via the Firebase Admin SDK. The Entity Relationship Diagram [see Fig. 5(b)] and Supplementary Video S1 illustrate how data are organized into collections and documents. The top-level collection (nodes) contains documents for each node dynamically created by the gateway when a new node joins the network. Each node document tracks status and information via multiple predefined fields created by the gateway and contains a subcollection (experiments) for experiments, where real-time amplification data and timestamps are stored individually for each test in arrays. Firestore's real-time update capability ensures that uploaded data is immediately available for dashboard visualization and spatiotemporal analysis, enabling timely decision-making in decentralized monitoring systems. The use of arrays to store time-series data reduces the number of read and write operations, as multiple time values can be updated in a single transaction. This efficient storage structure minimizes database overhead, making it highly advantageous for scaling the network to accommodate additional nodes and experiments. The hierarchical organization of data into collections and subcollections further enhances scalability by dynamically creating new documents for each node and experiment without requiring predefined schemas. A NoSQL database like Firestore is particularly well-suited for this application due to its flexibility in handling unstructured or semistructured data. Unlike traditional relational databases, which rely on fixed schemas, Firestore's document-based structure allows dynamic adaptation to new nodes, metadata fields, or experiment configurations.

To validate the network's performance under varying transmission conditions, four nodes were tested simultaneously to simulate realistic communication scenarios. The data transmission scenarios evaluated the impact of message overlap on network reliability, as illustrated in Fig. 5(c). In the first scenario, nodes transmitted sequentially, ensuring no message overlap. The second scenario introduced partial overlap, in which nodes were transmitted at fixed 20-s intervals but with staggered starts to create occasional collisions. The final scenario maximized overlap by all nodes transmitting simultaneously at 20-s intervals. To achieve the final scenario, transmissions were initiated for all nodes at the same time to the best of our ability. In all cases, an acknowledgment mechanism ensured retries for incompletely transmitted messages, with up to three retries per message.

The results demonstrate minimal message loss across all scenarios. In the sequential transmission scenario (see Fig. 5(c), left), a PDR of 99.6% was achieved, with two messages lost per node despite the lack of overlap. Introducing partial overlap (see Fig. 5(c), center) resulted in slight increases in message loss, with PDRs of 99.6% for two nodes and 99.3% for the others. Finally, the scenario with maximum overlap (see Fig. 5(c), right) showed a PDR of 99.6% for one node, 99.3% for two nodes, and 98.6% for the remaining one. Despite these small losses, no crosstalk between nodes or incorrect document assignments were observed. Notably, the minor message delivery losses had no discernible impact on the RT-LAMP amplification data. Sufficient data points were retained across all scenarios to accurately reconstruct reaction curves, demonstrating the system's robustness for real-time monitoring. The consistent message loss observed for Node_001 across scenarios may be due to its relative position to the gateway, which could affect signal strength.

D. Interactive Dashboard

Efficient data visualization and control interfaces are essential for decentralized monitoring systems, enabling real-time

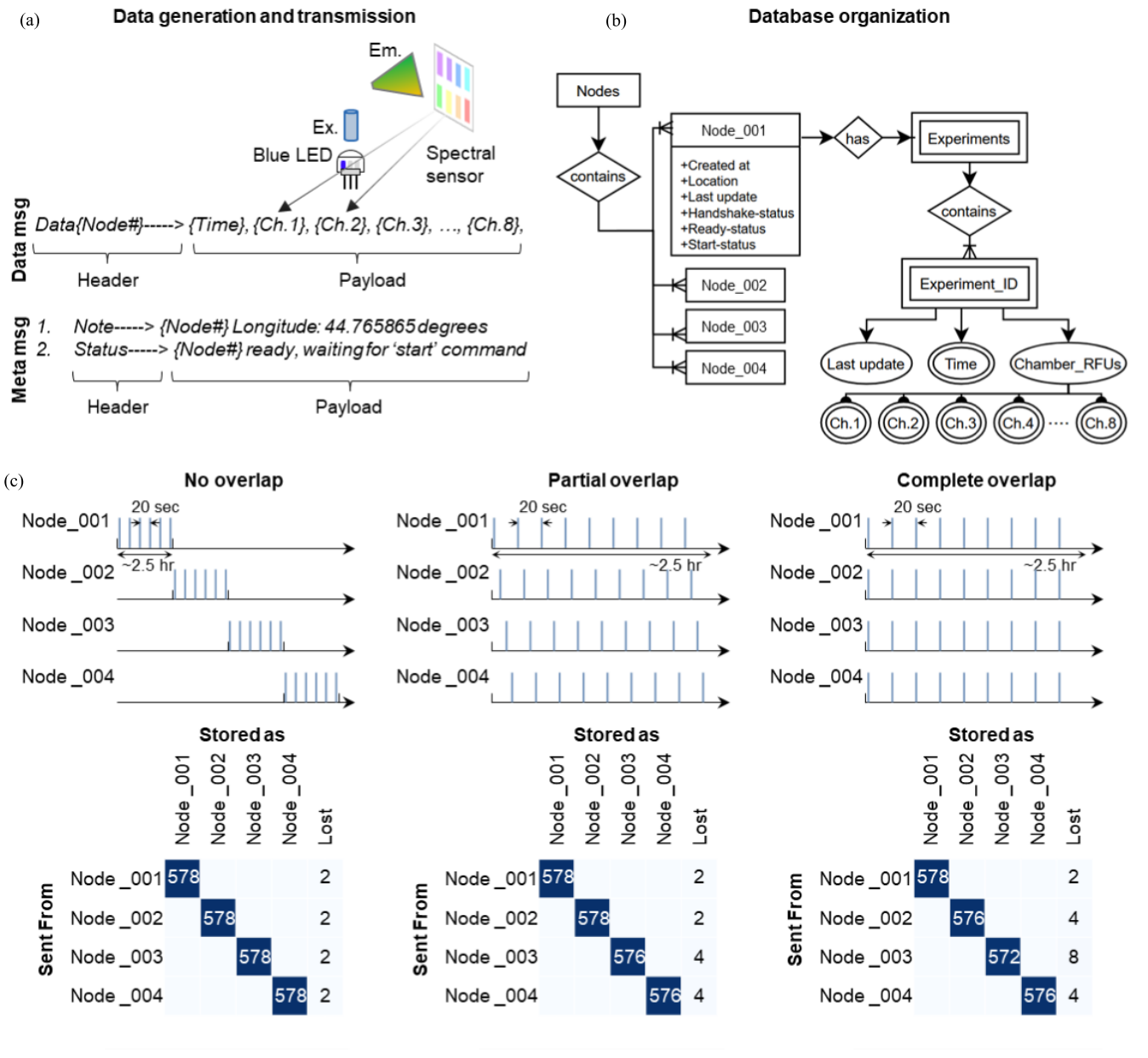

Fig. 5. Data generation, transmission, and network reliability. (a) Fluorescence emissions during the RT-LAMP reaction captured by a spectral sensor across eight wavelength channels are recorded as RFUs with timestamps every 20 s and transmitted with node ID as a data message. Meta messages include additional information, such as GPS coordinates and node status. (b) Entity relationship diagram illustrating the data organization in Google Firestore. A collection named "Nodes" contains dynamically assigned documents for each node when it joins the network by handshaking with the gateway. This parent document has fields to track the node status and contains a daughter subcollection of documents named "Experiments" for experiment-specific real-time amplification data. (c) Data transmission reliability under varying message overlap conditions. Sequential transmission achieves a PDR of 99.6%, with minimal message loss (left). Partial overlap, where nodes transmit at staggered intervals, results in slight message loss but maintains high PDRs of 99.3% and 99.6% (center). Maximum overlap, with all nodes transmitting simultaneously, yields PDRs of 99.6%, 99.3%, and 98.6% (right). Across all scenarios, no crosstalk or misassigned data was observed, and minor losses did not impact the reconstruction of RT-LAMP curves, demonstrating the system's robustness for real-time monitoring.

data interpretation and spatiotemporal analysis [44], [45]. To showcase these capabilities, a proof-of-concept dashboard was developed (see Supplementary Video V2 for a walkthrough of its operation). It integrates real-time data transmission, centralized storage, and geographic visualization, which are critical for supporting timely public health interventions and statistical analysis [46], [47]. The dashboard is programmed using Node.js and HTML—Node.js handles server-side scripting and interaction with Firebase, while HTML facilitates the graphical components. It is hosted directly on Firebase (https://aneksh-ionat.web.app/), which allows seamless integration with Firestore for data retrieval and updates, avoiding the need for dashboard-specific templates or third-party hosting tools. Unregistered users can access all data visualization features without logging in, while admin users (those with predefined credentials) can access additional control features related to the nodes. The dashboard is divided into two primary functionalities.

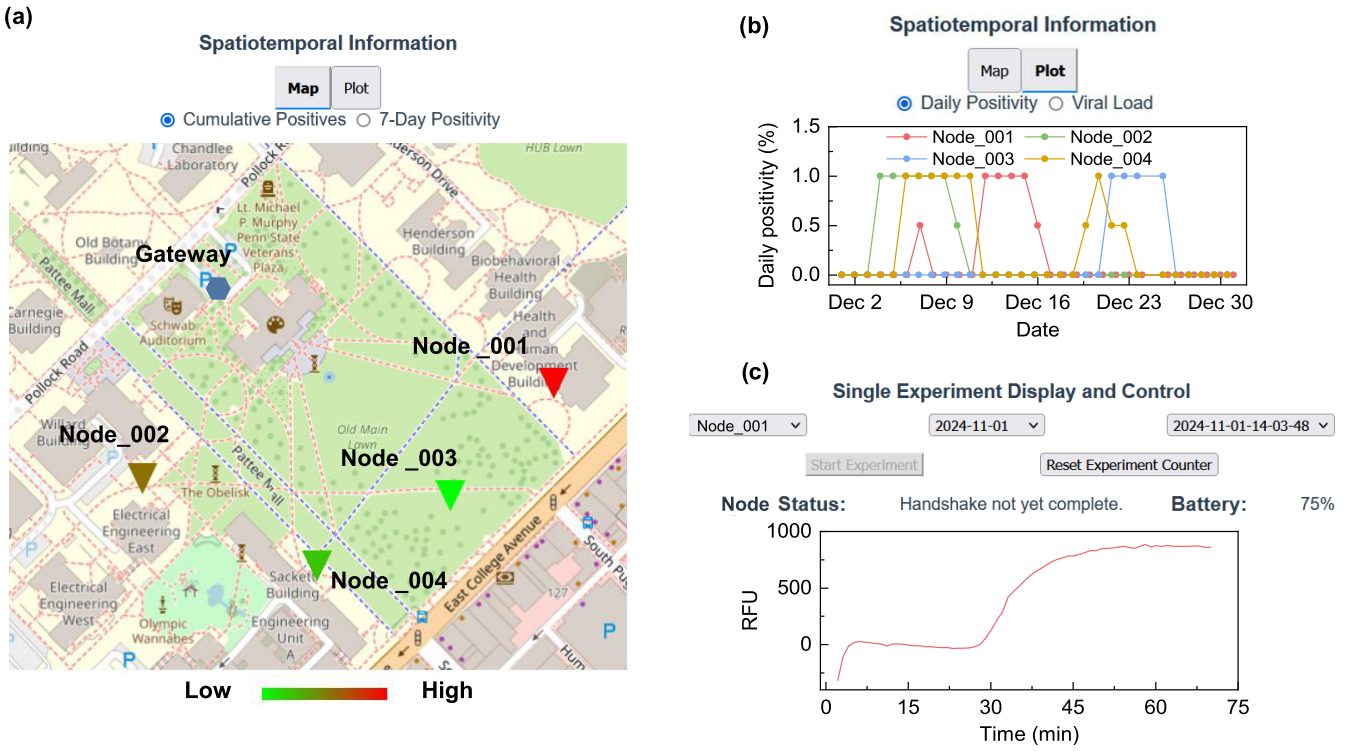

Fig. 6. Spatiotemporal visualization and experiment control on the interactive dashboard. (a) Nodes are displayed on a rendered map using GPS coordinates retrieved from their built-in GPS modules. Users can toggle between two data visualization modes: cumulative positive results and seven-day positivity rates, dynamically computed from mock experimental data in Firebase. Color-coded icons indicate positivity levels, enabling geographic trend analysis and hotspot identification. (b) Separate tab provides a temporal view, displaying datewise daily positivity rates. (c) Dashboard also allows interaction with ongoing and historical experiments for individual nodes. Users can select a node via a drop-down menu or by clicking its map icon. Real-time RFU time-series data is displayed for active tests, while historical data is accessible through additional menus. Admin users can initiate new experiments, reset experiment counters, or receive alerts when cartridge replacement or battery servicing is required, ensuring smooth and continuous operation in decentralized deployments.

1) *Spatiotemporal Information Visualization:* Nodes are displayed on a rendered map using GPS coordinates retrieved from their built-in GPS modules [see Fig. 6(a)]. Users can toggle between two selectable data visualization modes: cumulative positive results and seven-day positivity rates, which can be dynamically computed from mock experimental data stored in the respective documents of each node in Firestore. Color-coded icons on the map provide a quick representation of positivity levels, ranging from low to high, based on the selected mode [see Fig. 6(a)]. This enables users to identify geographic trends and potential hotspots. Alternatively, a separate tab [see Fig. 6(b)] allows the user to view a temporal plot, a line chart of daily positivity as a function of test dates. Under typical operation, one test is conducted daily, with a second confirmatory test performed if the first test is positive. Instances of 0.5 positivity observed could be either due to a false positive test or low viral load shed into the wastewater, which is near the assay's detection limit.
2) *Single Experiment Display with Control Options:* The dashboard also enables users to interact with ongoing or historical experiments for specific nodes. A node can be selected either from a drop-down menu or directly by clicking its icon on the map. If a test is actively running, its real-time amplification data, such as RFU time series, are displayed immediately [see Fig. 6(c)]. For completed experiments, users can retrieve historical data through additional drop-down menus. Admin users have the ability to start new experiments if the status fields indicate readiness or reset the experiment counter if the microfluidic cartridge has been replaced. In addition, the experiment counter or remaining battery percentage triggers alerts in the status field to notify operators when cartridge replacement or battery servicing is required. These features ensure smooth operation and reduce downtime for decentralized deployments.

The dashboard's design is well-suited for scaling up the number of nodes across larger geographic areas, providing centralized data aggregation and real-time insights. This minimizes the operational burden of visiting each location daily for manual sample collection or experiment monitoring. Instead, operators can manage and monitor the entire system remotely, streamlining workflows and enabling timely, data-driven public health interventions. By offering spatiotemporal analysis and seamless experiment control, the dashboard demonstrates its potential as a scalable and efficient tool for decentralized NAT-based monitoring networks, capable of supporting extensive applications in public health surveillance.

V. Conclusion and Future Perspective

We present a fully integrated and scalable networked NAT system, combining portable nodes with automated data

transmission to a centralized, interactive dashboard for real-time visualization and storage. The system supports direct on-site molecular testing while enabling spatiotemporal data aggregation, making it a powerful tool for decentralized pathogen monitoring and public health surveillance. Its scalable network architecture enables deployment of multiple nodes across larger geographic areas, significantly expanding testing coverage and facilitating monitoring without extensive manual intervention. This study demonstrates proof of concept by integrating and validating individual components using mock experimental data under controlled conditions. The results further demonstrate that molecular detection can be successfully integrated into low-power wireless IoT networks, enabling decentralized genomic surveillance without reliance on centralized laboratories. This approach has important implications for public health, where automated wastewater monitoring could provide early warning signals of emerging outbreaks and drive resource allocation. While detailed future research directions are outlined below, the broader impact of this work lies in illustrating how distributed, IoT-enabled molecular testing can transform population-level pathogen surveillance.

At the node level, operation is currently limited by the cartridge design, which supports only eight reactions before replacement, thereby constraining deployment to approximately one week. To enable extended deployments, we are pursuing a modular architecture that separates RNA enrichment and amplification modules and incorporates a robotic gantry to automate the transfer of consumables between them. This approach will allow individual tubes and silica columns to be swapped during operation, overcoming the limitations of a fixed multichamber cartridge. In parallel, upstream RNA enrichment will be integrated to improve sensitivity for low-abundance samples. These refinements, along with ongoing work on reagent lyophilization and stability and ruggedized housing, are intended to support month-long autonomous field operation.

We implemented direct LoRa communication between nodes and a single gateway, achieving a PDR above 99% during hour-long assays with four nodes. While adequate for demonstrating proof of concept, this architecture has several limitations for real-world deployment. Reliance on a single gateway creates a point of failure and constrains coverage, which may vary considerably in urban environments. In addition, our raw LoRa implementation does not include standardized security features such as device authentication or end-to-end encryption, which will be necessary for handling sensitive data. Finally, the current setup lacks redundancy; loss of the gateway or its backhaul would interrupt data transfer. Future work will, therefore, focus on developing a more robust architecture through multigateway coverage, relay, or multihop approaches to extend effective range, and incorporation of secure transmission protocols to ensure reliable and confidential operation in distributed wastewater surveillance.

Future deployment in real-world environments will require addressing multiple practical challenges. First, harsh environmental conditions such as temperature extremes, high humidity, and off-grid operation necessitate ruggedized design features. The outer enclosure will be fabricated from durable, UV-stabilized materials (e.g., glass-filled nylon or anodized aluminum) and sealed to an IP65 rating with continuous gaskets, stainless steel fasteners, and IP-rated connectors. Internal electronics will be protected by conformal coatings, desiccant packs, and environmental stress testing will be conducted to ensure resistance to moisture and dust. Second, connectivity might vary across geographic contexts, even though LoRa provides a multikilometer range in rural and low-infrastructure settings, urban deployments with higher interference may require multigateway coverage to ensure reliable communication. Finally, deployment at scale must comply with regional spectrum regulations and ensure secure transmission of sensitive health data, implemented through authentication and encryption mechanisms. By addressing these environmental, connectivity, and regulatory challenges, the system can transition from proof-of-concept to robust field-ready deployment.

Real-world testing remains a critical next step in system development. Our group has previously benchmarked portable amplification devices against gold-standard qPCR assays using contrived and clinical samples, including blood, plasma, nasal swabs, and saliva [22], [23], [25], [34]. This prior experience provides a methodological foundation for rigorous comparative evaluation of the presented platform. In future work, we plan to collaborate with environmental and public health researchers to perform parallel testing of wastewater samples with both our node and conventional qPCR/NGS workflows, enabling direct comparison of sensitivity, specificity, turnaround time, and operational requirements under real-world conditions.

ACKNOWLEDGMENT

Any opinions, findings, conclusions, or recommendations expressed in this work are those of the authors and should not be construed to represent any official NSF, NIH, USDA, or US Government determination or policy.

REFERENCES

[1] B. D. Kevadiya et al., "Diagnostics for SARS-CoV-2 infections," *Nature Mater.*, vol. 20, no. 5, pp. 593–605, May 2021, doi: 10.1038/s41563-020-00906-z.

[2] J. Peccia et al., "Measurement of SARS-CoV-2 RNA in wastewater tracks community infection dynamics," *Nature Biotechnol.*, vol. 38, no. 10, pp. 1164–1167, Oct. 2020, doi: 10.1038/s41587-020-0684-z.

[3] M. A. Johansson et al., "SARS-CoV-2 transmission from people without COVID-19 symptoms," *JAMA Netw. Open*, vol. 4, no. 1, Jan. 2021, Art. no. e2035057, doi: 10.1001/jamanetworkopen.2020.35057.

[4] T. R. Mercer and M. Salit, "Testing at scale during the COVID-19 pandemic," *Nature Rev. Genet.*, vol. 22, no. 7, pp. 415–426, Jul. 2021, doi: 10.1038/s41576-021-00360-w.

[5] A. L. García-Basteiro et al., "Monitoring the COVID-19 epidemic in the context of widespread local transmission," *Lancet Respiratory Med.*, vol. 8, no. 5, pp. 440–442, May 2020, doi: 10.1016/s2213-2600(20)30162-4.

[6] Y. Xu et al., "Characteristics of pediatric SARS-CoV-2 infection and potential evidence for persistent fecal viral shedding," *Nature Med.*, vol. 26, no. 4, pp. 502–505, Apr. 2020, doi: 10.1038/s41591-020-0817-4.

[7] W. Ahmed et al., "First confirmed detection of SARS-CoV-2 in untreated wastewater in australia: A proof of concept for the wastewater surveillance of COVID-19 in the community," *Sci. Total Environ.*, vol. 728, Aug. 2020, Art. no. 138764, doi: 10.1016/j.scitotenv.2020.138764.

[8] F. Saguti et al., "Surveillance of wastewater revealed peaks of SARS-CoV-2 preceding those of hospitalized patients with COVID-19," *Water Res.*, vol. 189, Feb. 2021, Art. no. 116620, doi: 10.1016/j.watres.2020.116620.

[9] W. Randazzo, P. Truchado, E. Cuevas-Ferrando, P. Simón, A. Allende, and G. Sánchez, "SARS-CoV-2 RNA in wastewater anticipated COVID-19 occurrence in a low prevalence area," *Water Res.*, vol. 181, Aug. 2020, Art. no. 115942, doi: 10.1016/j.watres.2020.115942.

[10] G. Medema, L. Heijnen, G. Elsinga, R. Italiaander, and A. Brouwer, "Presence of SARS-coronavirus-2 RNA in sewage and correlation with reported COVID-19 prevalence in the early stage of the epidemic in The Netherlands," *Environ. Sci. Technol. Lett.*, vol. 7, no. 7, pp. 511–516, Jul. 2020, doi: 10.1021/acs.estlett.0c00357.

[11] Y. Cao and R. Francis, "On forecasting the community-level COVID-19 cases from the concentration of SARS-CoV-2 in wastewater," *Sci. Total Environ.*, vol. 786, Sep. 2021, Art. no. 147451, doi: 10.1016/j.scitotenv.2021.147451.

[12] S. Karthikeyan et al., "Wastewater sequencing reveals early cryptic SARS-CoV-2 variant transmission," *Nature*, vol. 609, no. 7925, pp. 101–108, Sep. 2022, doi: 10.1038/s41586-022-05049-6.

[13] O. E. Hart and R. U. Halden, "Computational analysis of SARS-CoV-2/COVID-19 surveillance by wastewater-based epidemiology locally and globally: Feasibility, economy, opportunities and challenges," *Sci. Total Environ.*, vol. 730, Aug. 2020, Art. no. 138875, doi: 10.1016/j.scitotenv.2020.138875.

[14] D. Polo et al., "Making waves: Wastewater-based epidemiology for COVID-19—Approaches and challenges for surveillance and prediction," *Water Res.*, vol. 186, Nov. 2020, Art. no. 116404, doi: 10.1016/j.watres.2020.116404.

[15] T. Kumblathan, Y. Liu, G. K. Uppal, S. E. Hrudey, and X.-F. Li, "Wastewater-based epidemiology for community monitoring of SARS-CoV-2: Progress and challenges," *ACS Environ. Au*, vol. 1, no. 1, pp. 18–31, Nov. 2021, doi: 10.1021/acsenvironau.1c00015.

[16] J. Gonçalves et al., "Centralized and decentralized wastewater-based epidemiology to infer COVID-19 transmission—A brief review," *One Health*, vol. 15, Dec. 2022, Art. no. 100405, doi: 10.1016/j.onehlt.2022.100405.

[17] A.-M. Hokajärvi et al., "The detection and stability of the SARS-CoV-2 RNA biomarkers in wastewater influent in helsinki, Finland," *Sci. Total Environ.*, vol. 770, May 2021, Art. no. 145274, doi: 10.1016/j.scitotenv.2021.145274.

[18] *Wastewater Surveillance Testing Methods — National Wastewater Surveillance System — CDC*. Accessed: Jan. 15, 2025. [Online]. Available: https://archive.cdc.gov/www_cdc_gov/nwss/testing.html

[19] M. Kitajima et al., "SARS-CoV-2 in wastewater: State of the knowledge and research needs," *Sci. Total Environ.*, vol. 739, Oct. 2020, Art. no. 139076, doi: 10.1016/j.scitotenv.2020.139076.

[20] N. Alygizakis et al., "Analytical methodologies for the detection of SARS-CoV-2 in wastewater: Protocols and future perspectives," *TrAC Trends Anal. Chem.*, vol. 134, Jan. 2021, Art. no. 116125, doi: 10.1016/j.trac.2020.116125.

[21] F. Amman et al., "Viral variant-resolved wastewater surveillance of SARS-CoV-2 at national scale," *Nature Biotechnol.*, vol. 40, no. 12, pp. 1814–1822, Dec. 2022, doi: 10.1038/s41587-022-01387-y.

[22] A. Kshirsagar, G. Choi, V. Santosh, T. Harvey, R. C. Bernhards, and W. Guan, "Handheld purification-free nucleic acid testing device for point-of-need detection of malaria from whole blood," *ACS Sensors*, vol. 8, no. 2, pp. 673–683, Feb. 2023, doi: 10.1021/acssensors.2c02169.

[23] Z. Tang et al., "Rapid detection of novel coronavirus SARS-CoV-2 by RT-LAMP coupled solid-state nanopores," *Biosensors Bioelectron.*, vol. 197, Feb. 2022, Art. no. 113759, doi: 10.1016/j.bios.2021.113759.

[24] A. Kshirsagar, D. DeRosa, A. J. Politza, T. Liu, M. Dong, and W. Guan, "Point-of-need one-pot multiplexed RT-LAMP test for detecting three common respiratory viruses in saliva," *Biosensors Bioelectron.*, vol. 288, Nov. 2025, Art. no. 117836, doi: 10.1016/j.bios.2025.117836.

[25] T. Liu, A. J. Politza, A. Kshirsagar, Y. Zhu, and W. Guan, "Compact point-of-care device for self-administered HIV viral load tests from whole blood," *ACS Sensors*, vol. 8, no. 12, pp. 4716–4727, Dec. 2023, doi: 10.1021/acssensors.3c01819.

[26] C. Oh, G. Xun, S. T. Lane, V. A. Petrov, H. Zhao, and T. H. Nguyen, "Portable, single nucleotide polymorphism-specific duplex assay for virus surveillance in wastewater," *Sci. Total Environ.*, vol. 912, Feb. 2024, Art. no. 168701, doi: 10.1016/j.scitotenv.2023.168701.

[27] J. M. Boza et al., "Evaluation of a field deployable, high-throughput RT-LAMP device as an early warning system for COVID-19 through SARS-CoV-2 measurements in wastewater," *Sci. Total Environ.*, vol. 944, Sep. 2024, Art. no. 173744, doi: 10.1016/j.scitotenv.2024.173744.

[28] V. Sharma, H. Takamura, M. Biyani, and R. Honda, "Real-time on-site monitoring of viruses in wastewater using nanotrap particles and RICCA technologies," *Biosensors*, vol. 14, no. 3, p. 115, Feb. 2024, doi: 10.3390/bios14030115.

[29] E. González, J. Casanova-Chafer, A. Romero, X. Vilanova, J. Mitrovics, and E. Llobet, "LoRa sensor network development for air quality monitoring or detecting gas leakage events," *Sensors*, vol. 20, no. 21, p. 6225, Oct. 2020, doi: 10.3390/s20216225.

[30] J. Botero-valencia, L. Castano-Londono, D. Marquez-Viloria, and M. Rico-Garcia, "Data reduction in a low-cost environmental monitoring system based on LoRa for WSN," *IEEE Internet Things J.*, vol. 6, no. 2, pp. 3024–3030, Apr. 2019, doi: 10.1109/JIOT.2018.2878528.

[31] T. P. Lambrou, C. C. Anastasiou, C. G. Panayiotou, and M. M. Polycarpou, "A low-cost sensor network for real-time monitoring and contamination detection in drinking water distribution systems," *IEEE Sensors J.*, vol. 14, no. 8, pp. 2765–2772, Aug. 2014, doi: 10.1109/JSEN.2014.2316414.

[32] A. M. Alghamdi, E. F. Khairullah, and M. M. Al mojamed, "LoRaWAN performance analysis for a water monitoring and leakage detection system in a housing complex," *Sensors*, vol. 22, no. 19, p. 7188, Sep. 2022, doi: 10.3390/s22197188.

[33] S. J. Suji Prasad et al., "An efficient LoRa-based smart agriculture management and monitoring system using wireless sensor networks," *Int. J. Ambient Energy*, vol. 43, no. 1, pp. 5447–5450, Dec. 2022, doi: 10.1080/01430750.2021.1953591.

[34] Z. Tang et al., "SLIDE: Saliva-based SARS-CoV-2 self-testing with RT-LAMP in a mobile device," *ACS Sensors*, vol. 7, no. 8, pp. 2370–2378, Aug. 2022, doi: 10.1021/acssensors.2c01023.

[35] T. Notomi, "Loop-mediated isothermal amplification of DNA," *Nucleic Acids Res.*, vol. 28, no. 12, p. e63, Jun. 2000, doi: 10.1093/nar/28.12.e63.

[36] J. E. Ongerth and R. E. Danielson, "RT qLAMP—Direct detection of SARS-CoV-2 in raw sewage," *J. Biomolecular Techn.: JBT*, vol. 32, no. 3, pp. 206–213, Sep. 2021, doi: 10.7171/jbt.21-32-03-016.

[37] S. Westhaus et al., "Detection of SARS-CoV-2 in raw and treated wastewater in Germany—Suitability for COVID-19 surveillance and potential transmission risks," *Sci. Total Environ.*, vol. 751, Jan. 2021, Art. no. 141750, doi: 10.1016/j.scitotenv.2020.141750.

[38] A. Kshirsagar, A. J. Politza, and W. Guan, "Deep learning enabled universal multiplexed fluorescence detection for point-of-care applications," *ACS Sensors*, vol. 9, no. 8, pp. 4017–4027, Aug. 2024, doi: 10.1021/acssensors.4c00860.

[39] P. M. D'Aoust et al., "Quantitative analysis of SARS-CoV-2 RNA from wastewater solids in communities with low COVID-19 incidence and prevalence," *Water Res.*, vol. 188, Jan. 2021, Art. no. 116560, doi: 10.1016/j.watres.2020.116560.

[40] C. A. Robinson et al., "Defining biological and biophysical properties of SARS-CoV-2 genetic material in wastewater," *Sci. Total Environ.*, vol. 807, Feb. 2022, Art. no. 150786, doi: 10.1016/j.scitotenv.2021.150786.

[41] G. Mois, S. Folea, and T. Sanislav, "Analysis of three IoT-based wireless sensors for environmental monitoring," *IEEE Trans. Instrum. Meas.*, vol. 66, no. 8, pp. 2056–2064, Aug. 2017, doi: 10.1109/TIM.2017.2677619.

[42] H.-C. Lee and K.-H. Ke, "Monitoring of large-area IoT sensors using a LoRa wireless mesh network system: Design and evaluation," *IEEE Trans. Instrum. Meas.*, vol. 67, no. 9, pp. 2177–2187, Sep. 2018, doi: 10.1109/TIM.2018.2814082.

[43] P. Kulkarni, Q. O. A. Hakim, and A. Lakas, "Experimental evaluation of a campus-deployed IoT network using LoRa," *IEEE Sensors J.*, vol. 20, no. 5, pp. 2803–2811, Mar. 2020, doi: 10.1109/JSEN.2019.2953572.

[44] I. Dobraja and M.-J. Kraak, "Principles of dashboard adaptability to get insights into origin-destination data," *J. Location Based Services*, vol. 14, no. 1, pp. 28–48, Jan. 2020, doi: 10.1080/17489725.2020.1738577.

[45] S. Stehle and R. Kitchin, "Real-time and archival data visualisation techniques in city dashboards," *Int. J. Geographical Inf. Sci.*, vol. 34, no. 2, pp. 344–366, Feb. 2020, doi: 10.1080/13658816.2019.1594823.

[46] E. Dong, H. Du, and L. Gardner, "An interactive Web-based dashboard to track COVID-19 in real time," *Lancet Infectious Diseases*, vol. 20, no. 5, pp. 533–534, May 2020, doi: 10.1016/s1473-3099(20)30120-1.

[47] B. D. Wissel et al., "An interactive online dashboard for tracking COVID-19 in U.S. counties, cities, and states in real time," *J. Amer. Med. Inform. Assoc.*, vol. 27, no. 7, pp. 1121–1125, Jul. 2020, doi: 10.1093/jamia/ocaa071.

Aneesh Kshirsagar (Member, IEEE) received the B.Eng. degree in electronics and telecommunication from Savitribai Phule Pune University, Pune, India, in 2018, and the Ph.D. degree in electrical engineering from The Pennsylvania State University, University Park, PA, USA, in 2025.

He is currently a Post-Doctoral Fellow with Indiana University, Bloomington, IN, USA. He is the author of numerous published articles. His research interests include integrated biosensing instrumentation, point-of-care diagnostics, microfluidics, and translational multiomics.

Dr. Kshirsagar has been a Student Member of the Biomedical Engineering Society (BMES). His previous work has been recognized with the Best Paper Award from the IEEE Healthcare Innovations and Point of Care Technologies (HI-POCT) Conference in 2024.

Anthony J. Politza received the Ph.D. degree in biomedical engineering from The Pennsylvania State University, University Park, PA, USA, in 2025.

He was with The Pennsylvania State University at the time of this study and subsequenty joined Airbus US Space and Defense, Inc., State College, PA, USA. He is dedicated to using advanced diagnostic tools to eliminate barriers to medical care. His research interests include embedded molecular identification of high-risk viral infections, aiming to deliver simple, point-of-care testing that can be performed anywhere, with more than five years of experience in developing innovative devices, protocols, and system integrations for point-of-care technologies.

Ming Dong received the Ph.D. degree in electrical engineering from The Pennsylvania State University, University Park, PA, USA, in 2024.

He conducted research in solid-state nanopore fabrication and bio-sensing technologies. He was with The Pennsylvania State University at the time of this study and subsequently joined Huawei Technologies Company Ltd., Shanghai, China, as a Senior Thermal Engineer. His research focuses on nanopore based molecular diagnostics, including nucleic acid detection, saliva-based and airborne pathogen analysis, and signal transport mechanisms in nanoscale systems. His work integrates nanofabrication, materials characterization, and data analysis to develop sensitive and scalable biosensing platforms for point-of-care applications. He has contributed to multiple peer-reviewed publications in high-impact journals such as ACS Applied Materials & Interfaces, ACS Nano and Analytical Chemistry. His research has addressed applications ranging from CRISPR- and LAMP-based pathogen detection to nanopore-enabled analysis of disease-related biomarkers. Through his interdisciplinary training. He aims to advance accessible, accurate, and rapid molecular diagnostic technologies by combining solid-state devices with innovative sensing principles.

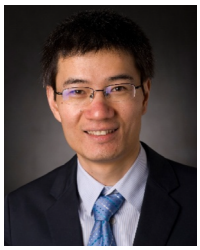

Weihua Guan (Senior Member, IEEE) received the Ph.D. degree in electrical engineering from Yale University, New Haven, CT, USA, in 2013.

He completed his postdoctoral training in biomedical engineering at Johns Hopkins University, Baltimore, MD, USA. He joined The Pennsylvania State University, University Park, PA, USA, where he held appointments in electrical engineering and biomedical engineering, and later moved to Indiana University Bloomington, Bloomington, IN, USA, where he is currently a Full Professor with the Department of Intelligent Systems Engineering. His research spans the interdisciplinary areas of molecular point-of-care testing, nanopore technology, embedded systems, edge computing, and artificial intelligence. His group develops biomedical sensors, devices, and integrated systems, along with new sensing principles and methods to advance molecular diagnostics and testing. His work aims to enable accessible, affordable, accurate, and actionable diagnosis wherever and whenever needed. He actively engaged in professional service and leadership.

Prof. Guan is an Active Member of BMES, SPIE, the Biophysical Society, and AAAS. His research has been recognized through multiple honors, including the HHMI International Research Fellowship and the NSF CAREER Award. He is a Frequent Reviewer for more than 40 high-impact journals and for federal funding agencies, including NSF and NIH.